MASTER'S THESIS

Evaluation and Characterization of a Logarithmic Image Sensor

LUND
UNIVERSITY

Author:

Sebastian FORS

Supervisors:

**Department of Measurement Technology and Industrial Electrical
Engineering, Division of Electrical Measurements**

Pelle OHLSSON

Axis Communications AB

Per WILHELMSSON

Niclas SVENSSON

Filip JOHANSSON

July 9, 2013

Abstract

In this thesis, issued by Axis Communications AB, a CMOS-type image sensor with a logarithmic response and wide dynamic range capabilities was evaluated and characterized with respect to signal response and noise characteristics. The evaluation was performed in the context of the need for wide dynamic range imaging in video surveillance. Noise characteristics were thoroughly evaluated with measurements performed with an integrating sphere. Additionally some aspects of temperature dependence of the device were investigated. The dynamic range was measured with a laser diffraction setup. The capability of the sensor to accurately capture motion was also investigated.

Acknowledgements

This thesis would not have been possible without the guidance and support of some of the people that I have met along the way. A sincere thanks to Per Wilhelmsson, Niclas Svensson and Filip Johansson, for initializing the thesis and for their support, guidance and great discussions.
I would also like to thank Anders Johannesson, for support, guidance and for sharing his knowledge in worthwhile discussions and comments, and Henrik Eliasson for valuable comments during the work with the thesis.

I want to thank my supervisor Pelle Ohlsson for valuable comments and for putting up with a somewhat chaotic hand-in schedule.

Finally a special thanks to all the people at Axis Communications that I have met while I have been working on this thesis and especially the people at the Department of Fixed Cameras/Fixed Domes for their companionship and support.

Contents

Acronyms

ADC analog-to-digital converter

ADU analog-to-digital units

CMOS complementary metal oxide semiconductor

DSNU dark signal non-uniformity

FFC flat-field correction

FPN fixed pattern noise

LED light emitting diode

MOSFET metal–oxide–semiconductor field-effect transistor

ND neutral density

PRNU photo response non-uniformity

RMS root mean square

ROI region of interest

SNR signal-to-noise ratio

WDR wide dynamic range

List of Figures

1 Introduction

1.1 Background

Axis Communications AB is a company that develops solutions for digital network based surveillance. These solutions include digital surveillance cameras. For a given surveillance scene you want to be able to capture all of the information in the scene, regardless of how dark or bright different parts of the scene are.

The differences between dark and bright parts of the scene make up the dynamic range. For instance, starlight amounts to an illuminance[1] of 10^{-3} lux while direct sunlight amounts to an illuminance of 10^5 lux [19].

Now, of course a scene with some parts lit by starlight and some by direct sunlight seems highly improbable. However in surveillance, it's not uncommon with scenes that encapsulates both dark indoor parts and bright outdoor parts. For instance, the entrance to a bank or a store. An example of such a scene rendered with a wide dynamic range (WDR) camera and a traditional camera can be seen in figure 1.

Figure 1: Left: WDR Camera, right: traditional Camera

The objects outside the entrance are illuminated by direct sunlight at 15000 lux, at the entrance the illuminance is 3000 lux and at the position close to the camera the illuminance is 300 lux. It's apparent from the image that the traditional camera struggles to render the entire scene accurately. To avoid overexposing the bright part, a fairly short exposure time is used which renders the dark parts noisy. The WDR camera manages to capture more of the information in the scene without over- or underexposing.

The aim of this thesis is to provide some insight into different methods of WDR imaging, particularly the use of complementary metal oxide semiconductor (CMOS) sensors with a logarithmic response in comparison to the use of multiple exposures.

---

[1]Wavelength-weighted measure that correlates with the wavelength-sensitivity of the eye.

1.2   CMOS Image Sensors

The CMOS-type image sensors commonly used today consists of a matrix of independent pixels. These pixels respond to light and give an analog electric output. This output is amplified and converted to a digital value with an analog-to-digital converter (ADC). The digital output of all pixels are sampled which provides the image data. The basic image sensor and pixel layout can be seen in figure 2.
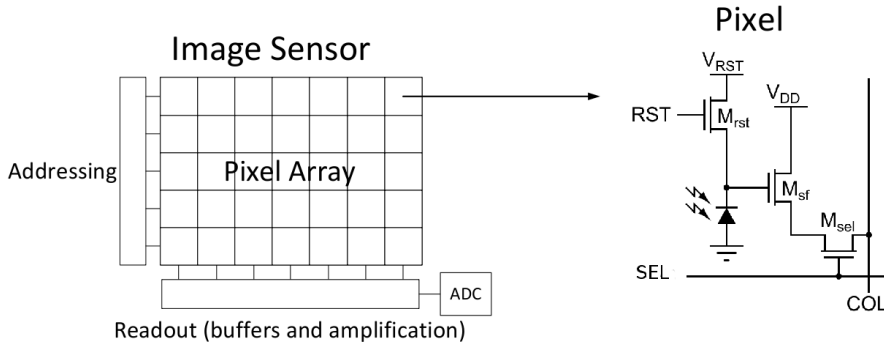
Figure 2: Traditional CMOS-type integrating pixel.

This pixel design is known as a 3T active pixel [16]. The basic operation is that the pixel is reset by a reset signal RST to an initial voltage V_{RST}. The photocurrent induced by illuminating the photodiode in the pixel discharges the photodiode capacitance. The residual voltage on the capacitance is then buffered and amplified by the second transistor M_{sf}. When the third transistor M_{sel} is activated via the selection signal SEL, the buffered voltage is read out to a column buffer where it can be amplified further and converted to a digital signal via an ADC. Additionally the active pixel usually allows for what is known as double sampling, sampling right after the reset to have a known reference signal used for noise subtraction.

In a CMOS-type sensor with a rolling shutter the sensor is read out pixel by pixel one row at the time. The selection signal SEL is then formed by three different signals, know as Pixel Clock, HSync and VSync. A schematic of these signals can be seen in figure 3.
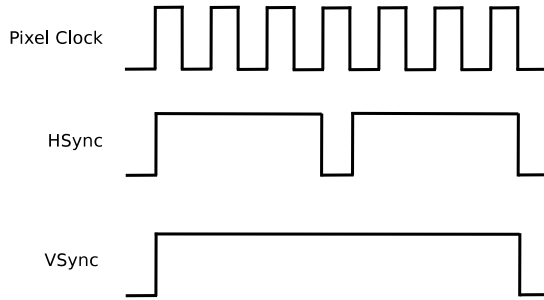
Figure 3: Image sensor readout timing signals.

The pixel clock is a high frequency pulse train that determines when a specific pixel is read out. The HSync signal determines when a certain row is read out and the VSync signal determines when a frame is active [3].

Additionally there is a reset signal that determines when the integration of a pixel is restarted. The active period of a pixel is known as the exposure time and it is during the exposure that the photocurrent discharges the pixel. If the pixel is completely discharged during the exposure time it has reached what is known as the pixel "full well" capacity. By changing the exposure time the pixel can be allowed to operate in different illumination conditions since the illumination determines how fast a pixel reaches its full well capacity [15]. A schematic of the read out pixel signal as a function of illumination can be seen in figure 4.
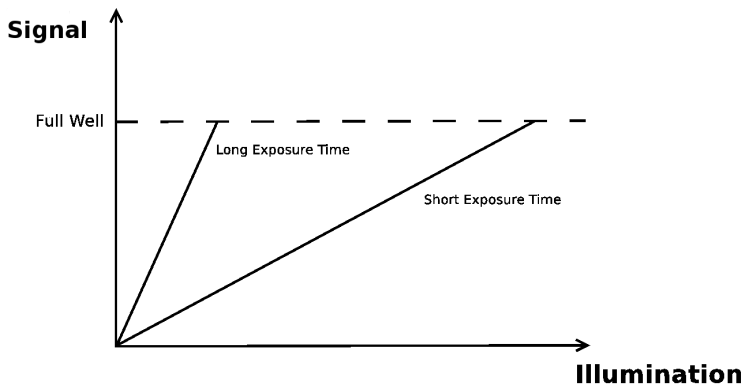
Figure 4: Integrating pixel read out signal as a function of illumination.

The pixel has a constant sensitivity to light but the exposure time allows control of the response in different conditions. A long exposure time means a high voltage, even at very low illumination levels. The downside is of course that full well is reached at a low illumination level. This means that the resulting image will be "burnt out" if parts of the scene illuminate the pixel to full well capacity.

However, if the exposure time is shortened, the illumination response will be less and even bright parts will be correctly represented in the final image but since the signal is small at low illumination levels, noise induced in the read out chain will affect the signal and in turn the resulting image.

For scenes with a dynamic range higher than the sensor is able to handle at a certain exposure level a choice has to be made by either burning out bright parts or having noisy dark parts.

Rolling Shutter   The read out scheme described in the previous section is known as a rolling shutter. This scheme has the effect that different parts of the sensor are exposed and read out at different times, usually in rows from top to bottom of the sensor.

This results in that a fast moving object might be captured incorrectly and the object will be distorted in the image, since some parts of the object are captured at different times than other parts. An example of this can be seen in figure 5.

Figure 5: Picture of moving fan, shows rolling shutter effect [1].

Color Filter Array   The most common way of achieving color imaging is by the use of a color filter array. The different pixels are covered with red,green and blue color filters in a pattern, usually a pattern known as the Bayer pattern, shown in figure 6. The color filter changes the pixel response to only respond to certain wavelengths. The missing colors for each pixel are then interpolated from the surrounding pixels to form the final color image [15].

Figure 6: Schematic of the color filter array pattern.

1.3 Dynamic Range and Dynamic Range Extension Techniques.

As mentioned in section 1.2, a CMOS-type image sensor is usually limited in how much difference between bright and dark parts of a scene that can be captured simultaneously. This limitation is known as the sensor dynamic range. The dynamic range mostly quoted for traditional CMOS sensors is somewhere in the range of 55-70dB [7] where the dynamic range is calculated according to equation (1),

$$DR = 20log\left(\frac{S}{N}\right) \tag{1}$$

where:
DR is the dynamic range in dB,
S is the saturation limit, i.e. voltage or digital Unit,
N is the noise floor, i.e. voltage or digital Unit.

Additionally, the ISO 15739 standard defines dynamic range as: "The ratio of the maximum luminance that receives a unique coded representation (the "saturation" luminance) to the lowest luminance for which the signal to noise ratio (SNR) is at least 1.0. This is based on the very arbitrary assumption that detail recorded with a SNR of 1.0 or above is useful and that recorded with an SNR less than 1.0 is not." [14]. Only temporal noise is considered for this measure.

When the dynamic range of a scene is very high an image sensor with a dynamic range in the range of 55-70dB can't capture all of the information in the scene and gives a picture with either burnt out parts or noisy and dark parts. This can be seen in figure 7.

Figure 7: Picture of scene with high dynamic range.

Dynamic Range Extension To remedy this limitation, a number of techniques and alternative pixel designs have been suggested [4, 22, 24, 26]. Specifically dual sampling [24] or even multiple sampling [4, 26] are techniques that have achieved some success and found its way into commercial products.

The basic principle is that each pixel is sampled multiple times with different exposure times that then are combined to provide an extended dynamic range.

This technique can provide excellent dynamic range but there are also drawbacks. Since we use multiple exposures, fast moving object might not be captured properly and "motion artifacts" can appear in the image. An example of this can be seen in figure 8.

Figure 8: Picture of object rotating a 30 rpm, left: one exposure, right: multiple exposures.

Furthermore, as shown by Yang and Gamal [25] the signal-to-noise ratio contains dips at certain points due to the use of multiple samples. This can cause different parts of the image having different noise characteristics, and even bright parts having more noise than dark parts.

Another technique that has been suggested is the use of sensors with a non-linear response, usually a logarithmic response. This technique has sometimes been described as a sensor technique that mimics the response of the human eye [21]. Section 1.4 covers the current state of logarithmic image sensors.

1.4 Logarithmic CMOS Sensors

MOSFET-based design

The concept of an image sensor with a logarithmic response is not new and is described in the literature [5, 20]. Most attempts in creating logarithmic image sensors share a common trait. They all achieve the logarithmic response by utilizing the characteristics of a metal–oxide–semiconductor field-effect transistor (MOSFET) in subthreshold mode.

The basic principle is the following. A photodiode is illuminated which induces a photocurrent. This photocurrent is converted into a logarithmically compressed voltage using a MOSFET in subthreshold mode which is then read out with a scheme similar to the one described in section 1.2. In most designs, the photocurrent is read out directly without any integration.

This design has been plagued by a number of inherent problems i.e. the lack of a zero reference, which means that when there is no photocurrent there is still a nonzero gate voltage on the MOSFET. Without any means of resetting the pixel before read out, variations of the pixels offset voltage have led to a very high FPN [13]. Additionally, residual charge on the photodiode from earlier readouts can cause image lag[2].

Design based on photodiode in photovoltaic mode

A different way of achieving a logarithmic pixel response, is to utilize the properties of a photodiode in photovoltaic mode. The proposed pixel design can be seen in figure 9.

The voltage on the photodiode is given by equation (2),

$$V_{pd} = \frac{kT}{q} ln(\frac{I_\lambda + I_s}{I_s}) \qquad (2)$$

where:

V_{pd} is the open circuit voltage on the photodiode,

k is Boltzmann's constant,

T is the temperature,

q is the elementary charge,

I_λ is the photocurrent,

I_s is the junction saturation current.

---

[2]Information from previous frames is present in the current frame even though the captured scene has changed.
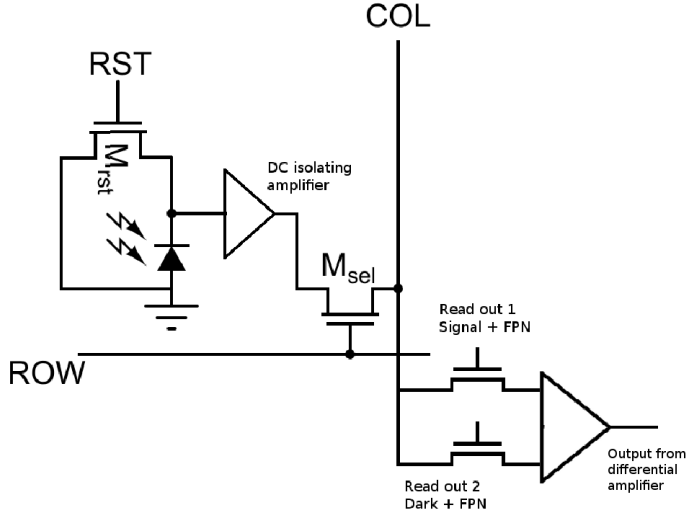
Figure 9: Logarithmic pixel utilizing photodiode in photovoltaic mode [27].

This design allows the pixel to be reset using the transistor denoted as M_{RST} in figure 9. The purpose of the reset is to remove residual charge on the photo diode, preventing image lag and to provide a reference signal use to subtract FPN from the output. The FPN subtraction is achieved by sampling the voltage before and after reset, the voltages are transferred to two column buffers and read out through a differential amplifier. This to remove offset variations in the pixel response.
Another effect of this design is the time it takes for the photo diode voltage to stabilize after the pixel reset. This is dependent on the illumination level and exposure time, giving a linear response at low illumination levels or short exposure times [27]. This linear response is given by equation (3),

$$V_{pd} = \frac{I_\lambda}{C_D} t \qquad (3)$$

where:
C_D is the photodiode junction capacitance,
I_λ is the photocurrent,
t is the exposure time.

The promises of this design is, much reduced FPN, increased low light sensitivity and no image lag [27].

1.5 Method and Approach

The goal of this thesis was to characterize and evaluate an image sensor with the photodiode-based pixel design described in section 1.4. The evaluation consisted of several parts, investigating the sensor performance from different perspectives. At the start of the thesis work, a number of hypotheses and suggestions for evaluations were put forward to be used as a basis for the measurements.

- What does the sensor response look like, at what illumination does the sensor saturate?

- Do the noise improvements claimed for the pixel design hold true?

- Is there a visible transition between logarithmic mode and linear mode?

- How does the sensor low light performance compare to traditional sensors?

- How do motion and light flicker in different lighting affect the sensor?

- How does this sensor compare to a multi-exposure solution for WDR imaging?

This thesis attempts to address and if possible answer these questions and hypotheses by measuring the sensor performance during different circumstances.

2 Measurement Setup

This section covers the measurement equipment used during the tests and the evaluation of the sensor. An integrating sphere was used to measure the sensor response and noise characteristics when illuminated. A climate chamber was used to characterize the sensor behavior when exposed to different ambient temperatures. A setup with a diode laser was used for dynamic range measurements. Another setup with a light emitting diode (LED) controlled by a micro controller was used to investigate the time-dependent behavior of the image sensor. For scene illumination measurements and sphere calibration, a light meter was used (Konica Minolta T-10).

2.1 Sensor and Data Acquisition

A sensor evaluation kit was obtained from the manufacturer. This kit contains the sensor with all the necessary electronics, including a 14-bit ADC, mounted off-chip but on the evaluation kit allowing the direct delivery of digital image data. The evaluation kit has a standard CS lens mount for use with different lenses. The evaluation kit utilizes a standard serial interface, CameraLink, which provides high-speed access to the image sensor data.

The sensor data was acquired using a PC laptop and frame grabber extension card with the same CameraLink interface. The frame grabber software allows for the capture of snapshots or image sequences of raw image data directly from the sensor evaluation kit. The images were acquired in 16-bit RAW format, using two bytes representing each pixel value. All measurements, except regular images for viewing purposes, were performed without optics. Figure 10 shows an overview of the basic setup.
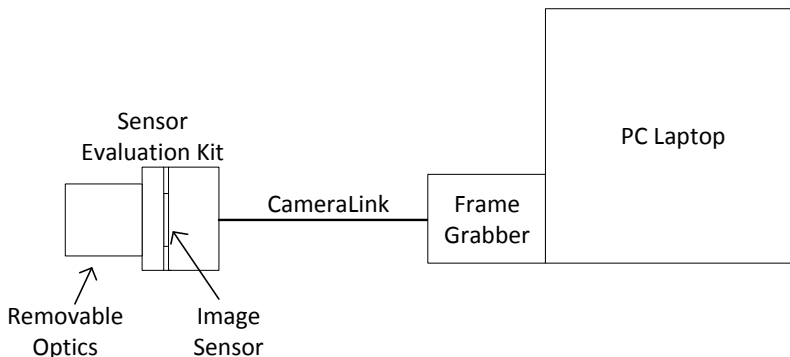
Figure 10: Schematic of basic measurement setup.

Processing of the image data was done in Python 2.5.2 [23] using the SciPy 0.6.0 [11], NumPy 1.1.0 [17] and Matplotlib 0.98.1 [10] modules.

2.2 Integrating Sphere

To evaluate the characteristics of an image sensor, the sensor must be uniformly illuminated with high precision and repeatability. This was accomplished by using an integrating sphere from SphereOptics. The integrating sphere was invented in 1892 by the British scientist W. E. Sumpner and provides a spatially uniform source of radiance[3] [18]. Figure 11 shows a schematic overview of the basic principle of the integrating sphere. Since the illuminance only depends on the sphere radius, different sensors can be mounted on the sphere and all measure the same amount of radiant light or illuminance.
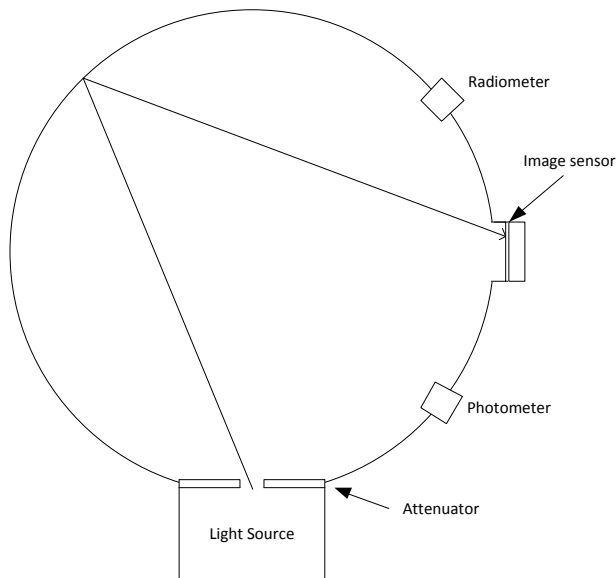
Figure 11: Schematic of integrating sphere.

The light source of the integrating sphere is a white halogen bulb. There are two ways of changing the amount of light entering the sphere. One way is to change the amount of current for the light source, although it is important to note that this changes the spectrum which in turn changes the photometer and radiometer values, since they have a certain spectral response. The second way to change the amount of light entering the sphere is via an attenuator with very fine control. The attenuator can be adjusted from fully open to fully closed with an accuracy of 0.001%.

---

[3] A measure of the amount of electromagnetic radiation leaving or arriving at a point on a surface.

The sphere has two different sensors, a radiometer[4] and a photometer[5]. These sensors produce a current that is registered by the sphere control software. The sensors are not calibrated to any exact quantity of light but provide a relative measure of the light intensity for comparisons between different sensors. For the purpose of presenting measurements with a relatable quantity an external light meter (Konica Minolta T-10) was used to "calibrate" the sphere sensors to illuminance values when the sphere was used at different settings. Figure 12 and 13 shows the Light Meter response as a function of the sphere photometer and radiometer respectively on a loglog-scale. Each figure shows three separate measurements at 20%, 50% and 100% of maximum sphere lamp voltage. According to the sphere control software, this corresponds to approximately 1%, 16% and 100% of the maximum sphere lamp output.
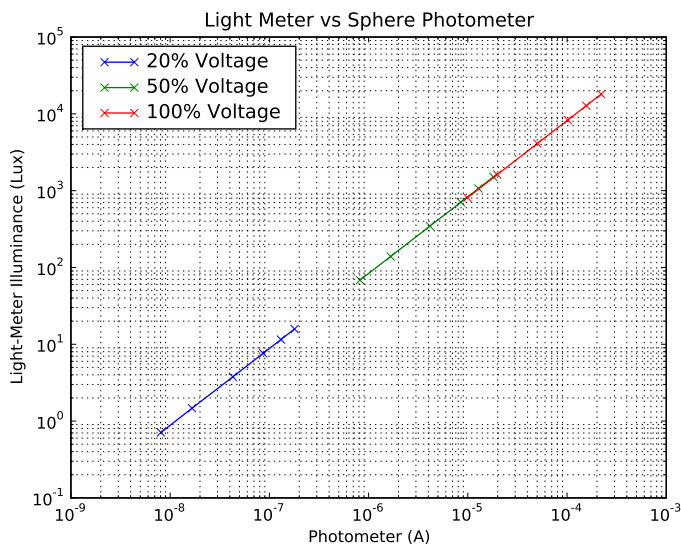
Figure 12: Light meter response as a function of photometer response.

---

[4]Measures the power of the electromagnetic radiation.
[5]A radiometer with a filter, to match human vision.
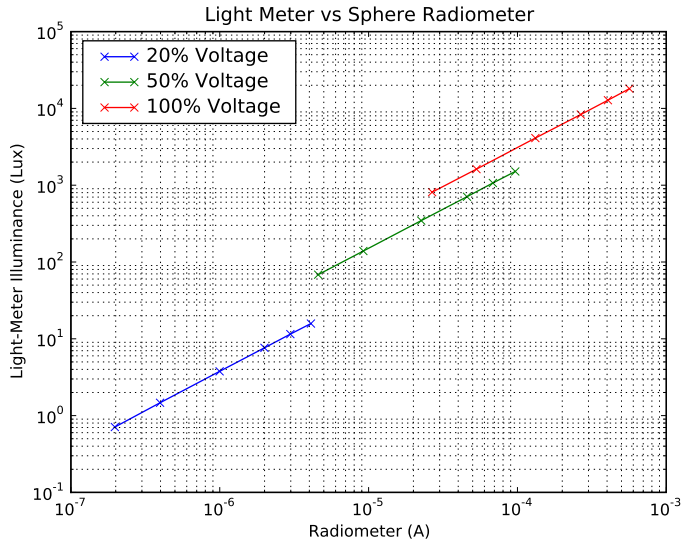
Figure 13: Light meter response as a function of radiometer response.

As can be seen in figure 12 the photometer response is linear with the light meter response over the different settings. The radiometer response seen in figure 13 is linear within the different measurements but the response is different when the sphere lamp voltage changes. Due to the higher signal values for the radiometer, for this thesis, the measured relations between the light meter illuminance and the radiometer current will be used to convert the measured light intensity to illuminance values.

2.3 Climate Chamber

For the purpose of evaluating how products perform in different temperatures, Axis Communications owns a number of climate chambers. The climate chamber used for temperature measurements in this thesis allows for temperatures in the range of $5°C$ to $60°C$ with a step size of $0.1°C$.

When performing temperature measurements, it is important to make sure that the temperature of the device under test is stable when data is acquired. This was accomplished by mounting a temperature probe on the evaluation kit and logging the temperature during one measurement.

The temperature dependence of both dark signal and noise characteristics was measured. The sensor was completely covered by mounting the optics with a closed iris and covering the entire evaluation kit with a piece of dark cloth. The sensor temperature was allowed to stabilize for two hours at each temperature level. Only completely dark frames were acquired.

2.4 Laser Diffraction

To measure the dynamic range of the image sensor, a setup that allows for both incredibly bright and very dark illumination of the sensor at the same time, is needed. This might be hard to achieve accurately in a lab setup with conventional lighting of a scene. Wang *et al.* [7] have suggested an alternative approach utilizing Fraunhofer diffraction from a circular aperture.
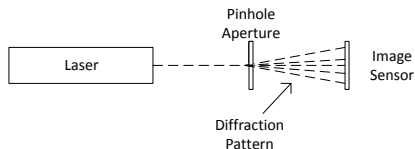
Figure 14: Schematic of laser diffraction measurement setup.

Figure 14 shows a schematic of the setup.

The test setup consists of: A laser, in this case a green laser with a wavelength of $532nm$ and an output power of $5mW$ and a pinhole aperture with a radius of $50\mu m$. The pinhole aperture is placed in front of the sensor which is then illuminated by the laser beam. This creates a diffraction pattern with known theoretical properties that can be used to determine the dynamic range of the sensor.

2.5 Blinking LED

For the purpose of evaluating the sensor response to flickering illumination and fast transitions between dark and bright illumination, a small setup with a LED and a micro-controller was built. This setup can be seen in figure 15.
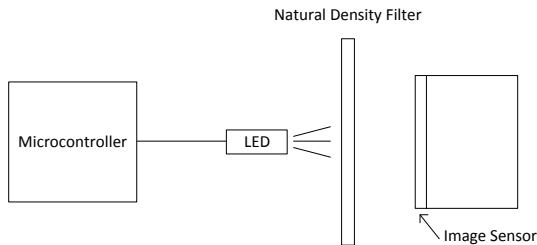
Figure 15: Schematic of LED flicker setup.

The entire setup was covered when measurements were performed to eliminate external light sources that might affect the result. For the purpose of changing the amount of light reaching the sensor the setup allows for the placement of neutral density (ND) filters between the LED and the sensor.

3 Measurement Theory

3.1 Signal Characteristics

3.1.1 Dark Signal Characteristics

A common starting point for image sensor evaluations is to acquire a number of completely dark images, by covering the sensor and making sure that no light reaches it. This data can then be used to evaluate a number of different parameters.

Firstly, the data can be used to exclude pixels with a vastly different response and/or behavior than all the other pixels, since the main interest is the average behavior of the image sensor. It is also important to make sure that the evaluation sample is in working condition and not defect in any way.

Secondly, the data can be used to assess the characteristics of the dark signal. If there is any offset from zero or if the signal is clipped at a certain level.

3.1.2   Illumination Response

When evaluating the signal characteristics of an image sensor, there are several important aspects to consider. Since the main function of the image sensor is to convert light into a digital signal, detailed measurements of the response to changes in the amount of light reaching the sensor needs to be performed.

This can be achieved using the integrating sphere setup described in section 2.2. The basic procedure is to mount the sensor to the integrating sphere, making sure that the only light illuminating the sensor is the light from the sphere.

The amount of light reaching the sensor is changed by gradually closing the sphere attenuator. At each discrete light level a number of frames are captured from the sensor. For a detailed description of the number of frames and illuminance levels used for the measurements in this thesis, please find Appendix A.

When performing measurements with illumination it is important to consider the effect of the image sensor's color filters described in section 1.2. Since all light sources have a certain spectral distribution and the color filters have different spectral response the response over the different color channels might differ. To account for this the different color channels can be separated according to figure 16.
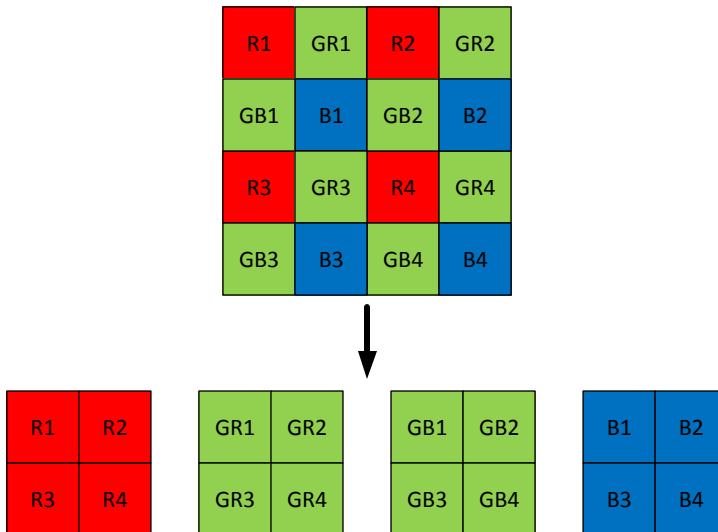
Figure 16: Schematic of color channel separation.

Theoretically the response of the green pixels on rows with blue and red pixels should be the same. Usually they are still treated as independent channels since the response might differ due to optical and/or electrical pixel crosstalk[6].

---
[6]Neighboring pixels influencing the response of a certain pixel.

The response can either be presented as the averages of the different color channels or as the average of all color channels. Additionally to measure the average response, both temporal noise and FPN described in section 3.2 must be reduced to achieve an accurate measure. This is done by a combination of spatial and temporal averaging. First, a number of consecutive frames are averaged in time as described by equation (4). This gives a single frame with reduced temporal noise:

$$\bar{p}_N(x,y) = \frac{1}{N} \sum_{i=1}^{N} p(x,y,i) \tag{4}$$

where:
N is the number of averaged frames,
$p(x,y,i)$ is the pixel value at pixel, (x,y) in frame i.

Secondly the FPN is reduced by averaging over the region of interest in the single frame according to equation (5),

$$\bar{p}_{N,ROI} = \frac{1}{M_{xy}} \sum_x \sum_y \bar{p}_N(x,y), \{x,y \in ROI\} \tag{5}$$

where:
N is the number of averaged frames,
$\bar{p}_N(x,y)$ is given by (4),
ROI is the set of pixel coordinates of the region of interest used,
M_{xy} is the total number of pixels in the region of interest.

To be able to calculate a signal without the dark signal offset, after each sphere measurement a set of dark frames were acquired. The average dark signal was calculated in the same way as the average signal.

3.2 Noise Characteristics

The noise in an image sensor is comprised of two main parts that will be referred to as temporal noise and FPN.

As the name implies, temporal noise is noise that changes from frame to frame. Common sources of this are: pixel reset noise and MOS device noise. Additionally in integrating sensors, photon shot noise is another source of temporal noise [2]. Visually in the image, temporal noise can be seen as flickering pixels in a stream of images.

Fixed pattern noise is noise that is stationary with respect to time. FPN is visible as patterns in otherwise homogeneous areas in the image, either in a random fashion or as vertical or horizontal lines due to mismatches between pixels or mismatches between different signal parts of the readout chain [2]. A schematic of how this can appear in the final picture can be seen in figure 17.
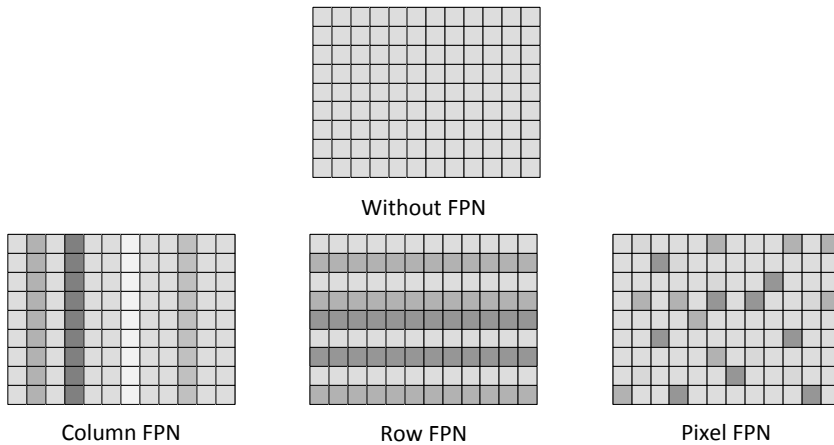
Figure 17: Schematic of row level, column level and pixel level FPN.

3.2.1   Temporal Noise

A common way of measuring the temporal noise, or root mean square (RMS) noise as it is also referred to, is to record two frames, subtract them and calculate the standard deviation with a correction factor [8]. To improve the statistics one may instead measure the average variations of all pixels on a frame to frame basis. Such a measure can be defined as:

$$\bar{\sigma}_{temporal} = \frac{1}{M_{xy}} \sum_x \sum_y \sigma_{temporal}(x, y), \{x, y \in ROI\} \tag{6}$$

$$\sigma_{temporal}(x, y) = \sqrt{\frac{1}{N} \sum_{i=1}^{N} (p(x, y, i) - \bar{p}_N(x, y))^2} \tag{7}$$

where:
N is the number of captured frames,
$p(x, y, i)$ is the pixel value at pixel (x, y) in frame i,
$\bar{p}_N(x, y)$ is the average value at pixel (x, y) over N frames,
ROI is the set of pixel coordinates of the region of interest used,
M_{xy} is the total number of pixels in the region of interest,

This measure describes the average pixel to pixel variations of the sensor in the region of interest.

3.2.2   Fixed Pattern Noise

The simplest way of modelling FPN is to assume a simple gain/offset variation type model which can be defined according to equation (8),

$$p(x, y) = a(x, y) + b(x, y)f(i) \tag{8}$$

where:
$p(x, y)$ is the response of a pixel at coordinates (x, y),
$a(x, y)$ is the offset of the pixel at coordinate (x, y),
$b(x, y)$ is the gain of the pixel at coordinate (x, y),
$f(i)$ is a function describing the ideal pixel response to illumination i.

The pixel offset is known as dark signal non-uniformity (DSNU) and the pixel gain is known as photo response non-uniformity (PRNU).

If the model described in equation (8) holds true, the standard deviation of two different pixels as a function of the average signal will take the form described in figure 18.
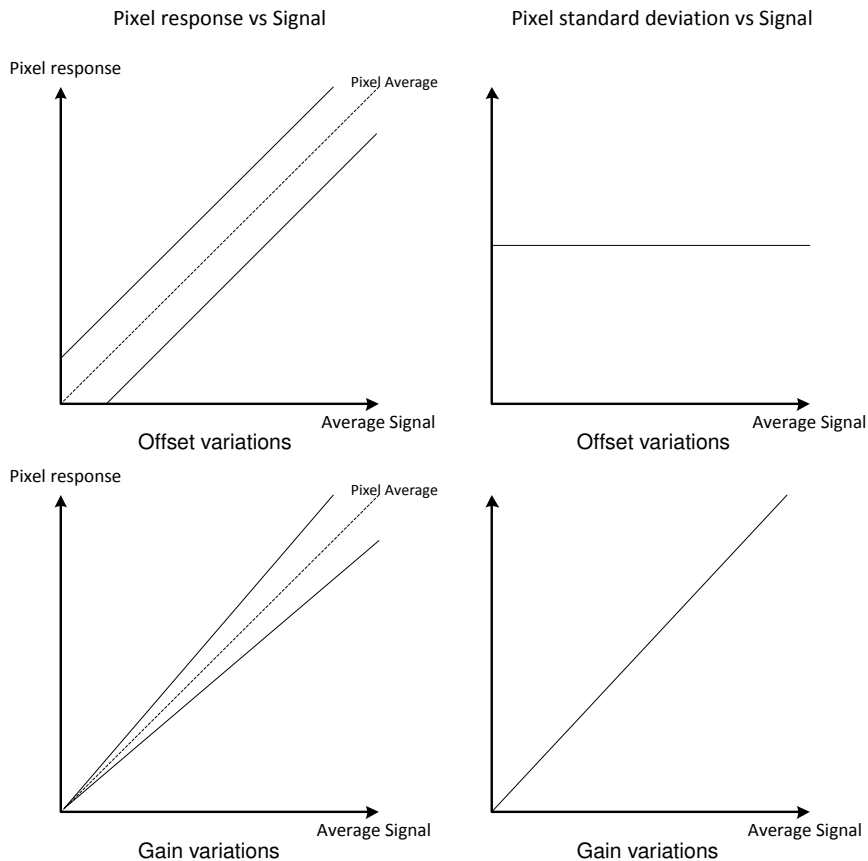
Figure 18: Overview of how offset and gain variations affect the FPN measures.

As can be seen in figure 18, if two different pixels have the same response but a difference in offset, the standard deviation of the pixels as a function of the average signal will be constant but different from zero.

If the pixels have a different response but no offset, the standard deviation will increase linearly as function of the average signal. A combination of both offset and gain variations will therefore result in an increasing standard deviation with a constant offset from zero. All FPN measures defined in this report relies on the use of standard deviation. Therefore if the model described in equation (8) holds, the measured FPN will show the same behavior as shown in figure 18.

To measure the FPN, the temporal noise must be removed. This is done by averaging in the same fashion as described in section 3.1.2.

Total Fixed Pattern Noise   There are different measures for the FPN, the simplest one includes all types of FPN in a single measure and is defined as:

$$\sigma_{TotalFPN} = \sqrt{\frac{1}{M_{xy}} \sum_x \sum_y (\bar{p}_N(x,y) - \bar{p}_{N,ROI})^2}, \{x,y \in ROI\} \qquad (9)$$

where:
N is the number of averaged frames,
$\bar{p}_N(x,y)$ is the average pixel value over N frames at pixel, (x,y), given by (4),
$\bar{p}_{N,ROI}$ is the average pixel value of the region of interest over N frames,
ROI is the set of pixel coordinates of the region of interest used,
M_{xy} is the total number of pixels in the region of interest.

This measure gives a value of the total variations of the pixels of the sensor.

Row and Column FPN   Another FPN measure is to measure the variations on a column basis, this can be defined as:

$$\sigma_{ColumnFPN} = \sqrt{\frac{1}{M_x} \sum_x (\bar{p}_{N,y}(x) - \bar{p}_{N,y})^2}, \{x,y \in ROI\} \qquad (10)$$

$$\bar{p}_{N,y}(x) = \frac{1}{M_y} \sum_y \bar{p}_N(x,y), \{x,y \in ROI\} \qquad (11)$$

where:
N is the number of averaged frames,
$\bar{p}_N(x,y)$ is the average pixel value over N frames at pixel, (x,y), given by (4),
$\bar{p}_{N,y}$ is the average value of the average column $\bar{p}_{N,y}(x)$ over N frames,
ROI is the set of pixel coordinates of the region of interest used,
M_x is the total number of rows in the region of interest,
M_y is the total number of columns in the region of interest.

This measure gives a value of the variations among the columns of the sensor.

Similarly the row FPN can be defined by exchanging the row and column indices:

$$\sigma_{RowFPN} = \sqrt{\frac{1}{M_y} \sum_y (\bar{p}_{N,x}(y) - \bar{p}_{N,x})^2}, \{x, y \in ROI\} \quad (12)$$

$$\bar{p}_{N,x}(y) = \frac{1}{M_x} \sum_x \bar{p}_N(x, y), \{x, y \in ROI\} \quad (13)$$

where:

N is the number of averaged frames,

$\bar{p}_N(x, y)$ is the average pixel value over N frames at pixel, (x, y), given by (4),

$\bar{p}_{N,x}$ is the average value of the average row $\bar{p}_{N,x}(y)$ over N frames,

ROI is the set of pixel coordinates of the region of interest used,

M_x is the total number of rows in the region of interest,

M_y is the total number of columns in the region of interest.

This measure gives a value of the variations among the rows of the sensor.

Pixel FPN The remaining FPN component not included in either the row or column FPN is the pixel FPN . This is the variations in pixel gain and offset that can't be accounted for by row and/or column variations. To measure this quantity the column and row FPN must be removed. This is done by averaging all rows with respect to an average row and all columns to an average column. Since this removes all row and column variations the remaining pixel FPN can be calculated in the same fashion as the total FPN given in equation (9). This gives the pixel FPN as:

$$\sigma_{PixelFPN} = \sqrt{\frac{1}{M_{xy}} \sum_x \sum_y (\bar{p}_{N,norm}(x, y) - \bar{p}_{N,norm,ROI})^2}, \{x, y \in ROI\} \quad (14)$$

$$\bar{p}_N(x, y)_{norm} = \left(\bar{p}_N(x, y) \cdot \frac{\bar{p}_{N,x}}{\bar{p}_{N,x}(y)} \right) \cdot \frac{\bar{p}_{N,y}}{\bar{p}_{N,y}(x)} \quad (15)$$

where:

N is the number of averaged frames,

$\bar{p}_{N,norm,ROI}$ is the average pixel value of the region of interest over N frames normalized with respect to column and row variations,

$\bar{p}_{N,y}$ is the average value of the average column $\bar{p}_{N,y}(x)$ over N frames,

$\bar{p}_{N,x}$ is the average value of the average row $\bar{p}_{N,x}(y)$ over N frames,

$\bar{p}_{N,y}(x)$ is given by (11),

$\bar{p}_{N,x}(y)$ is given by (13),

ROI is the set of pixel coordinates of the region of interest used,

M_x is the total number of rows in the region of interest,

M_y is the total number of columns in the region of interest.

3.3 Signal-to-noise Ratio

The signal-to-noise ratio (SNR) is a common measure of how high quality the output of certain system is. This can be used as a comparative measure between different imaging systems and is defined as:

$$SNR = \frac{s}{\sigma} \tag{16}$$

where:
s is the average signal,
σ is the temporal noise, in this case the standard deviation of the signal.

The SNR is often expressed as a power ratio according to:

$$SNR = 20log_{10}\left(\frac{s}{\sigma}\right) \tag{17}$$

3.4 Dynamic Range

Using the setup described in section 2.4, a diffraction pattern can be projected onto the image sensor surface. The intensity distribution of this diffraction pattern is given by equation (18) [9],

$$I(\theta) = I_0 \left(\frac{2 J_1(ka \cdot sin(\theta))}{ka \cdot sin(\theta)} \right)^2 \tag{18}$$

where:

I_0 is the intensity of the main peak,

J_1 is the first order Bessel function,

$k = \dfrac{2\pi}{\lambda}$ is the wavenumber, where λ is the wavelength,

a is the radius of the aperture,

θ is the angle of observation.

This relation allows us to theoretically calculate the relative intensities of the peaks in diffraction pattern. This information can then be used to determine the dynamic range of the sensor.
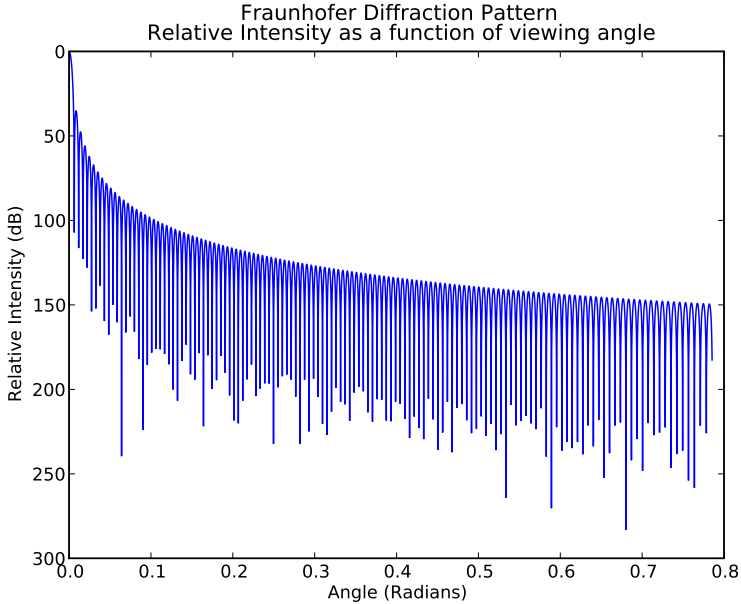
Figure 19: Theoretical intensity as a function of angle, $\lambda = 532$nm, a $= 50\mu$m.

Figure 19 shows the normalized intensity distribution as a function of the angle of observation θ. The angular distribution is however not of any importance when it comes to measure the dynamic range.

Instead we want to know the relative intensity dynamic range as a function of the peak number. This can be seen in figure 20.
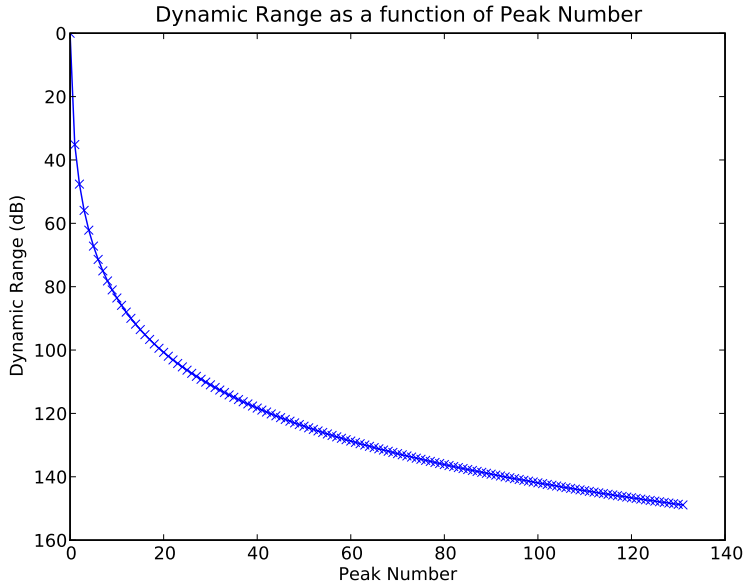
Figure 20: Dynamic Range as a function of peak number, $\lambda = 532$nm, a $= 50\mu$m.

The measurement is carried out by changing the laser intensity to a point just below sensor saturation. The dynamic range is then given by the smallest detectable peak in the image. Wang *et al.* [7] proposes this to be done by observation of the image. An alternative approach is to use the ISO definition of dynamic range mentioned in 1.3.

3.5 Transient Response

The image sensor under evaluation is not an integrating sensor as a traditional image sensor described in section 1.2. Therefore it might be interesting to try to characterize the transient response when an LED is turned on and off. The measurements can be used to reason about the sensor behavior in different situations and how the final image might be affected. As a comparison the response of a traditional integrating image sensor can be seen in figure 21.

Figure 21: Schematic of the transient response of an integrating image sensor.

For simplicity a theoretical line sensor with only 3 different rows is assumed. The upper part of the figure shows how the rows are read out after each other in a rolling shutter type fashion as described in section 1.2. The illumination as a function of time is also shown as an LED is turned on and off.

The lower part shows the values when the rows are read out. Since the rows are integrating the light during the integration period, the final value is only dependent on the how long the LED was lit during the integration period. This leads to the read out response seen in the lower part of the figure.

If a shorter integration/exposure time was used, the slope of the output signal would be steeper. If a longer integration/exposure time was used, the slope would be flatter. This, since a longer integration/exposure time would mean more pixels being active during the illumination increase and vice versa, assuming that the read out time is constant. This is also assuming that the LED response is fast enough to be considered step-like.

The transient behavior of the logarithmic sensor under evaluation was unknown and was measured and compared to the response of a traditional integrating sensors. The measurement was done by using the setup described in section 2.5. The LED was turned on and off repeatedly and at the same time a number of frames were recorded. The frames that were recorded during the LED on and off periods were extracted from the data set.

To reduce the amount of data and remove noise, the pixel response was averaged for each row and the rows were then plotted after each other leading to an output form identical to the one in figure 21. Additionally the rows were normalized with respect to the illumination profile and the maximum value. This since the response time is the main point of interest. Additionally the row response was filtered with a median filter and an averaging filter to provide a more clear signal without noise. As mentioned in section 1.4 the response of the pixel in the logarithmic sensor under evaluation is illumination dependent. Therefor the response with different ND filters was investigated.

ND filters are usually quantified by their optical density which is defined according to equation (19),

$$d = -log_{10}\left(\frac{I}{I_0}\right) \tag{19}$$

where:

d is the optical density,

I is the intensity after the filter,

I_0 is the incident intensity.

4 Results and Discussion

This section contains all the measurement results from the measurements performed as described in section 3.

4.1 Signal Characteristics

4.1.1 Dark Signal Characteristics

As described in section 3.1.1, the sensor evaluation kit was completely covered and 100 frames were acquired.
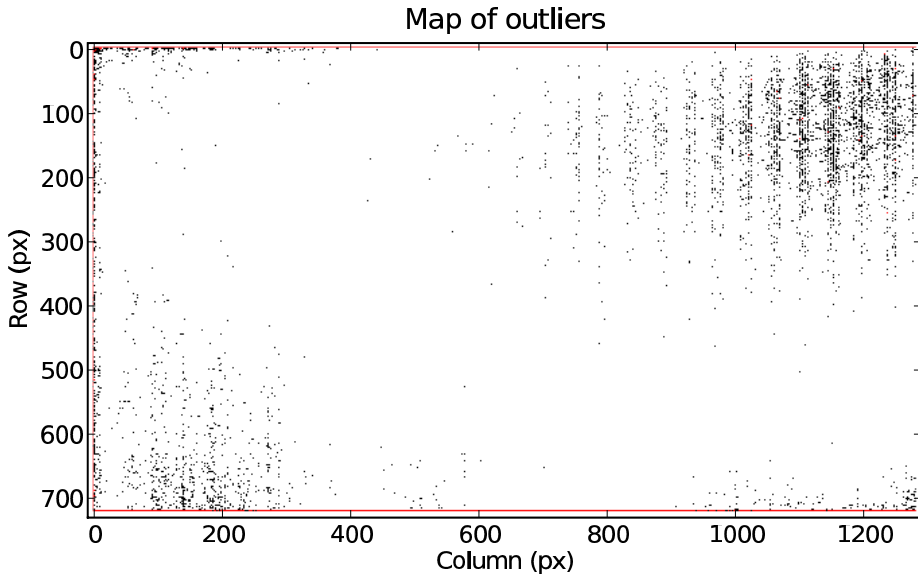
Outliers

Figure 22: Map of outlier pixels, ambient temperature: $25°C$.

Figure 22 shows a map of outlier pixels. The temporal noise has been removed by averaging in accordance with section 3.1.2. As can been seen in the figure, there are rows and columns at the edges of the sensor which contain pixels that are more than 3 standard deviations above or below the sensor mean. For this reason, a centered region of interest (ROI) denoted ROI_1 of 710 rows and 1270 columns was selected for use in some of the measurements. This was done to avoid that "bad" rows and columns influence the measurements to much. In the figure it can also be seen that there are scattered pixels with values above or below 2 standard deviations, these were not excluded from the measurements.
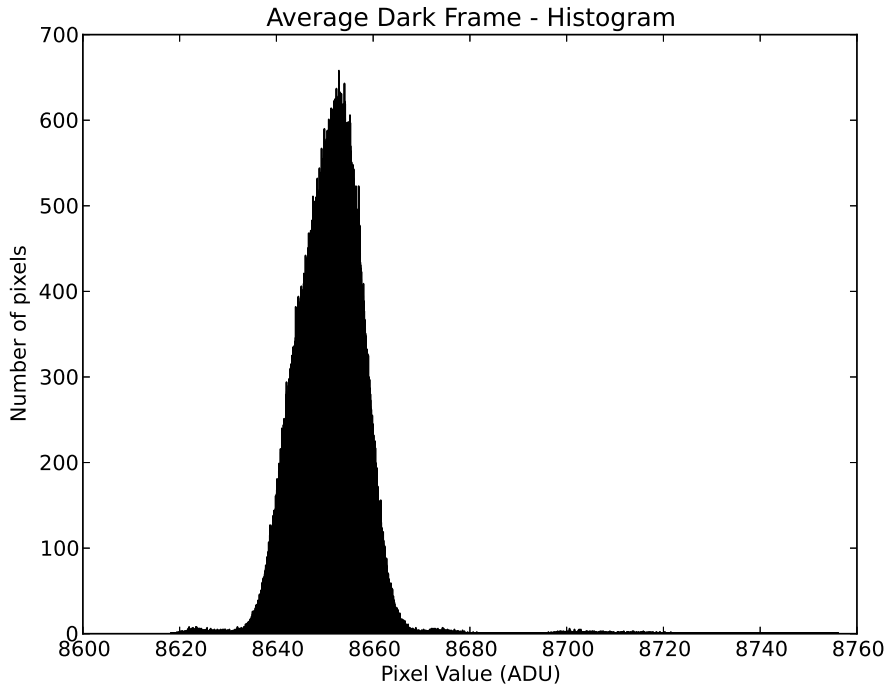
Histogram

Figure 23: Histogram of average dark frame, ambient temperature: $25°C$.

As can be seen in figure 23 there is no clipping of the histogram and the pixel values seem to be more or less evenly distributed around the mean.
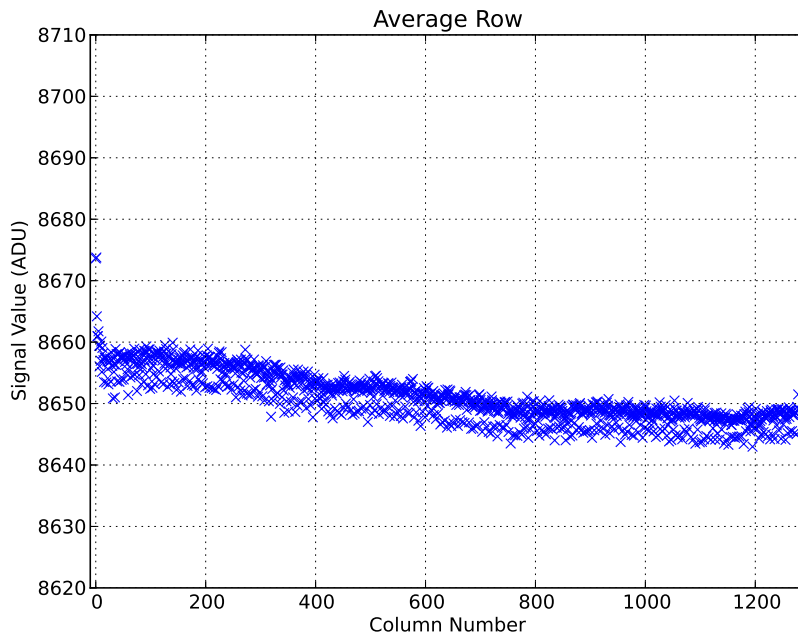
Average Row and Column

Figure 24: Average row at $25°C$

Figure 24 shows the values of a representative row. What this actually shows are the variations of the different columns of the image sensor. As can be seen there seems to be consistent variations between different columns that have the effect of creating two separated populations of column values. Additionally there seems to be a small gradient across the columns. Also the first few columns seem to have a different offset than the other ones, although these will be excluded when ROI_1 is used.
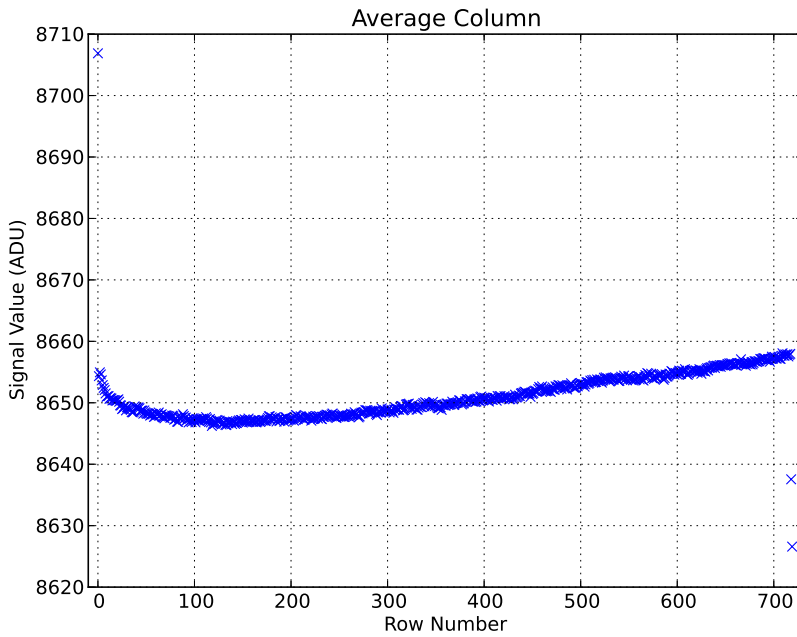
Figure 25: Average column at $25°C$

Figure 25 shows the values of a representative column. This shows the variations of the different rows of the image sensor. The scale is the same as in figure 24 and it's apparent that the variations from row to row is less than the column to column variations seen in figure 24. Additionally a small gradient across the rows can be seen. The first and last rows seem to have a different offset then most of the other rows, these are excluded in ROI_1.

Noise measures

Using the measures defined in section 3.1.2 and section 3.2 and ROI_1 the signal and noise without any illumination at an ambient temperature of $25°C$ can be seen in table 1.

Signal	Total FPN	Column FPN	Row FPN	Pixel FPN	Temporal Noise
8650.95 (ADU)	5.85 (ADU)	3.79 (ADU)	3.23 (ADU)	3.07 (ADU)	10.08 (ADU)

Table 1: Table of signal and noise measurements of dark frames, ROI_1.

As can be seen in table 1 the average signal of a completely dark frame is 8650.95 analog-to-digital units (ADU). This seems to be a quite high offset value considering that a 14-bit ADC is used on the evaluation kit. Essentially this means that only half the ADC range is used. Depending on the signal response this still leaves about 8000 digital steps remaining of the ADC output which should be enough for most applications.

Furthermore the FPN values cited in table 1 is essentially the DSNU since the sensor is not illuminated. The values seem quite low, especially considering the high offset values usually quoted for logarithmic image sensors. It is apparent that the presence of a reset as described in section 1.4 is an effective way of removing pixel offset. The row and column FPN is about the same, although the row FPN is dominated by a gradient and the column FPN is dominated by column to column variations.

The temporal noise is about 10 ADU which clearly dominates over the FPN at no illumination.

4.1.2 Illumination Response

As described in section 3.1.2 the illumination response measurements were performed using the integrating sphere setup described in section 2.2.
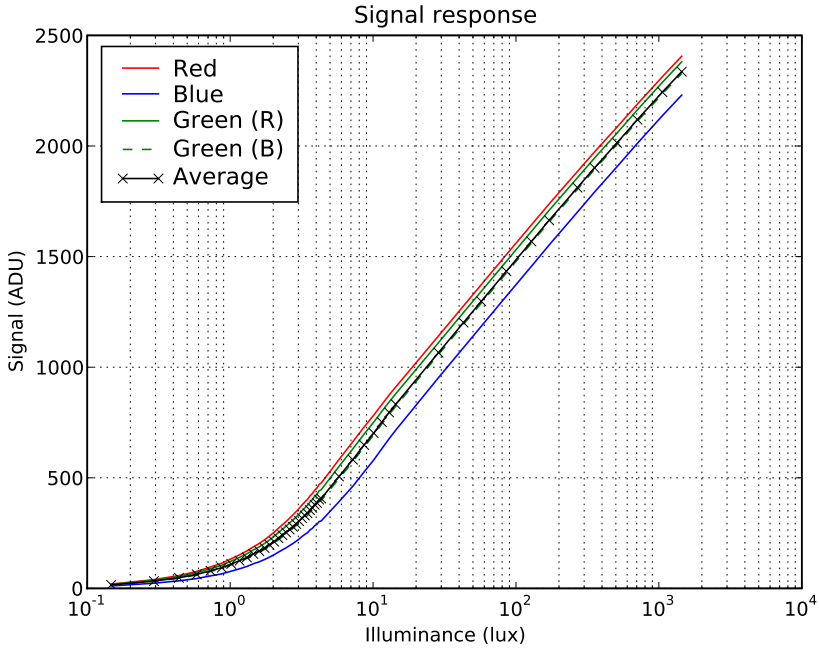

Figure 26: The average sensor signal with dark offset removed, plotted against the illumination, ROI_1, measurement A.1.

Figure 26 shows the signal response in a plot with a logarithmic x-scale. The responses of the different color channels are similar although a bit offset from each other due to different amounts of attenuation and the spectral distribution of the sphere light source.

Figure 27 shows the average signal of all color channels versus illumination with a line fitted to the 25 first datapoints and logarithm fitted to the last 15 data points.
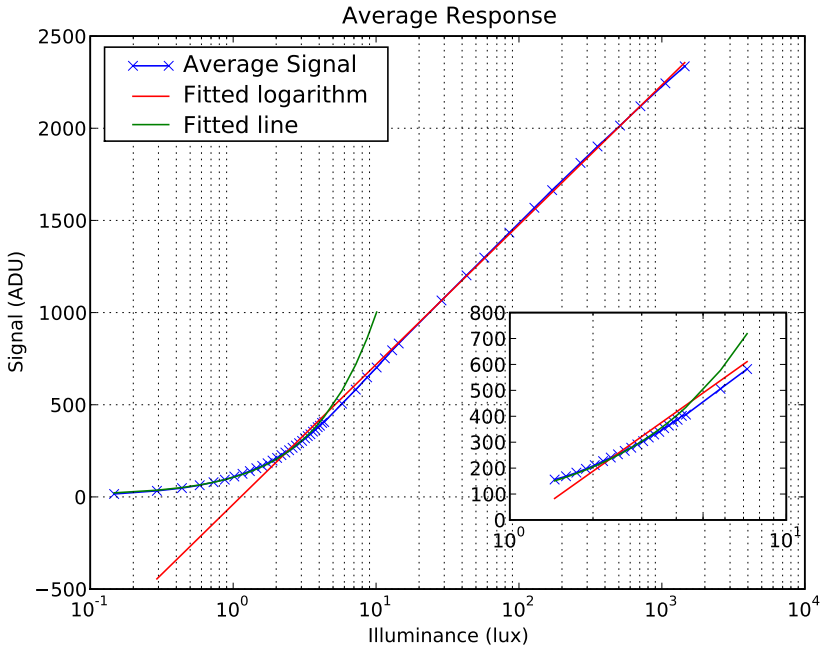

Figure 27: The average sensor signal with dark offset removed, with fitted logarithm and line, ROI_1, measurement A.1.

As can be seen in figure 27 at light levels above 10-20 lux the average response follows an almost perfect logarithmic relationsship with respect to illumination. At illumination levels below 2-3 lux the relationship between signal and illumination instead follows a linear relationship.
As can be seen in the zoomed in section of the plot, the transition between linear and logarithmic mode seem to happen somewhere between 3-10 lux. Although in this range the response is neither perfectly linear nor perfectly logarithmic.

4.1.3 Temperature dependence

The temperature dependence of the noise and dark signal was measured in accordance with section 2.3. At each temperature, 100 frames were acquired. Two separate measurements were performed to verify the consistency of the temperature dependent behavior.
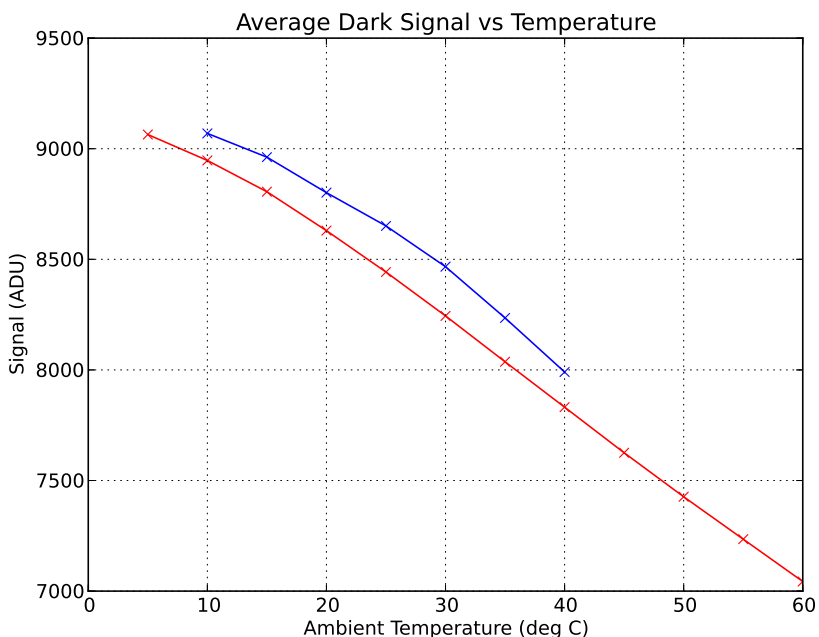
Figure 28: Average dark signal versus the ambient temperature, ROI_1.

Dark Signal

Figure 28 shows the average dark signal versus temperature. The apparent offset between the two measurements could be due to a slight difference in the stabilization time allowed. Another possible factor is the way the evaluation kit was covered with cloth, since this could possibly isolate the evaluation kit more or less.

As can be seen there is a substantial decrease in the average signal when the temperature is increased. This is a problematic result from an implementation point of view, since surveillance cameras need to be able to operate in different environments and in varying temperatures. The dark signal determines what is black in the image and if a predefined offset is used, the error could become quite large if the temperature changes, thus affecting the final image quality.
The average signal almost seems to decrease linearly with the signal so it is possible that a temperature dependent offset correction could be implemented.
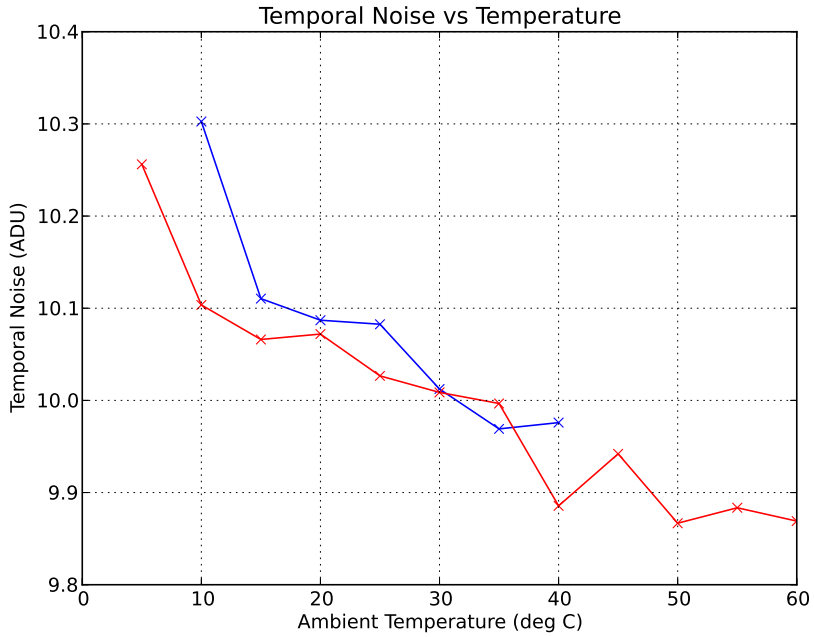
Noise

Figure 29: Temporal noise versus the ambient temperature, ROI_1.

Figure 29 shows the temporal noise versus temperature. As in the previous section, there is a slight offset between the two measurements. Observing the y-axis one can see that the variations of the temporal noise are incredibly small, and more or less constant over the entire temperature range. From an implementation point of view, this is a very good result since it means no apparent increase in temporal noise will be seen in the final image even at high temperatures.
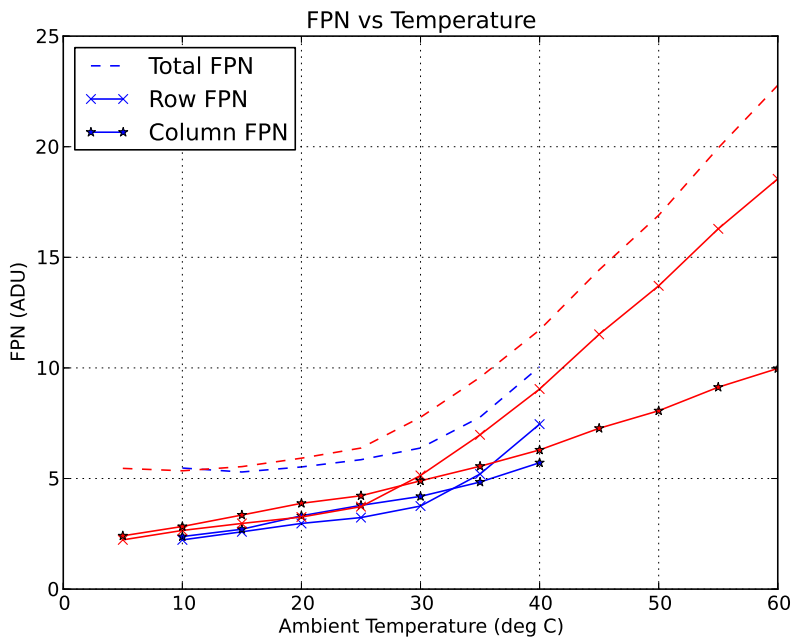
Figure 30: FPN versus the ambient temperature, ROI_1.

Figure 30 shows the total FPN and the row FPN versus the ambient temperature. Again the same offset between the measurements as before is visible. The FPN increases when the temperature increases. And as can be seen in the figure, the row FPN seems to be the dominant factor in the increase.

To determine the behavior of the FPN, the average row and column at $0°C$ and $60°C$ can be seen in figure 31 and 32.
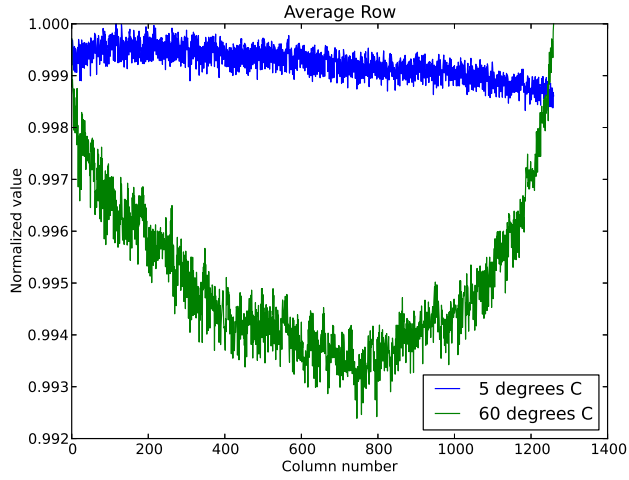
Figure 31: Normalized average row at two different temperatures, ROI_1.
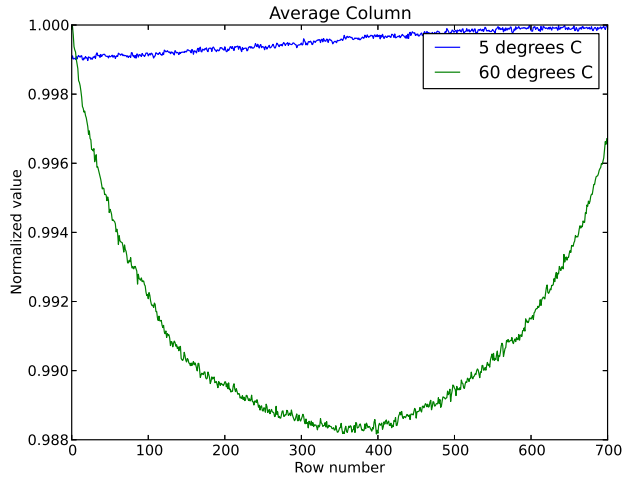
Figure 32: Normalized average column at two different temperatures, ROI_1.

As can be seen in figure 31 and 32. As the temperature increases the variations among the rows and columns increase. Both among the column and the rows there is a variation that seems to give lower signal values at the center and higher at the edges. Among the column there is also variations on a column to column level, such variations can be seen in the image as a stripy pattern as mentioned in section 3.2.

Summary

The temperature dependence measurements show both positive and negative results from an implementation point of view. The large change in dark signal is as mentioned problematic for a stable implementation. The constant temporal noise is a good result since this type of noise is hard to completely remove in the final image. The FPN increases with temperature but is still relatively low and if needed some form of correction scheme including temperature could potentially be devised.

4.2   Noise Characteristics

4.2.1   Temporal Noise

The temporal noise was measured in accordance with the description in section 3.2.

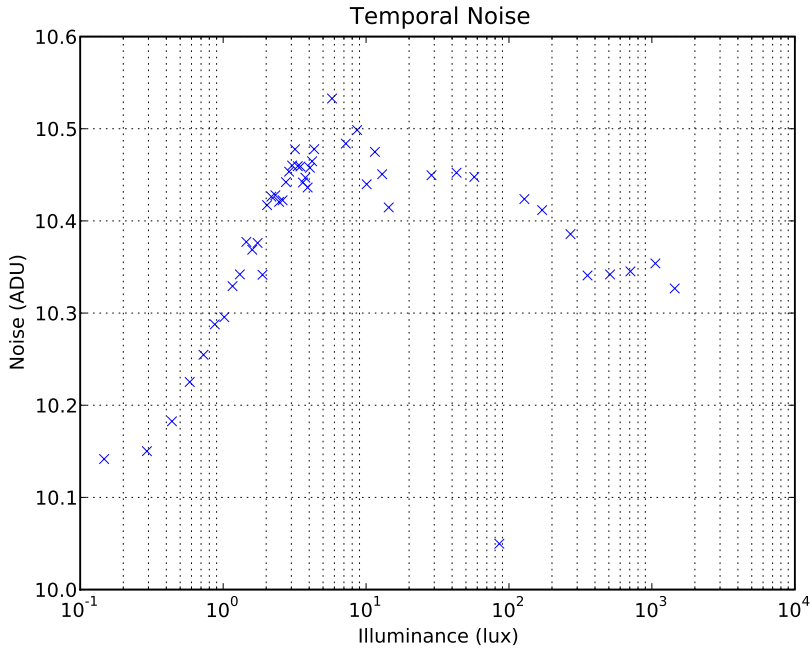Figure 33: The sensor temporal noise plotted versus the illuminance, measurement A.1.

Figure 33 shows the temporal noise versus the illumination. The noise does seem to remain fairly constant with the illumination as the variations are extremely small. Possibly a slight increase can be observed up to 10 lux.
One data point at 90 lux seems to be a bit off from the others, although it is still within one ADU of the other data points.

4.2.2 Fixed Pattern Noise

The FPN was measured in accordance with the description in section 3.2.2.
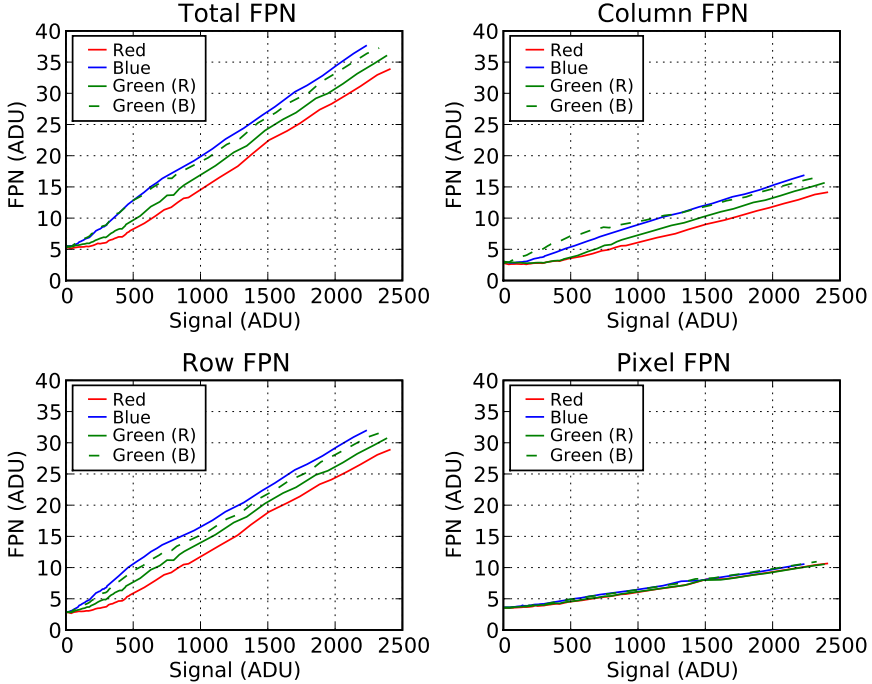
Figure 34: The FPN versus illumination per color channel measurement, ROI_1 A.1.

Figure 34 shows the FPN versus the sensor's average signal, for each color channel. The FPN model described in 3.2.2 seems to hold, as the FPN increases more or less linearly with the signal. The overall FPN is also fairly small compared with the signal which increases much faster. Since the row and column FPN, and in particular the row FPN seems to influence the total FPN the most it might be interesting to study the average row and column profiles at different illumination levels to see how the noise increases. This can be seen in figure 35 and 36.

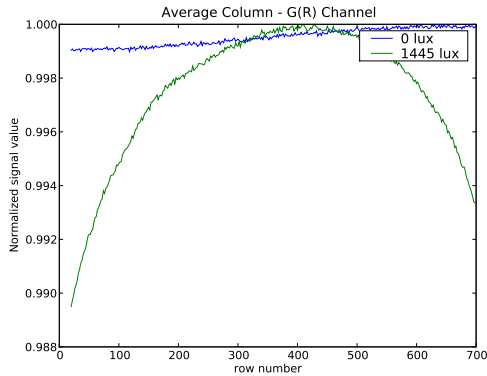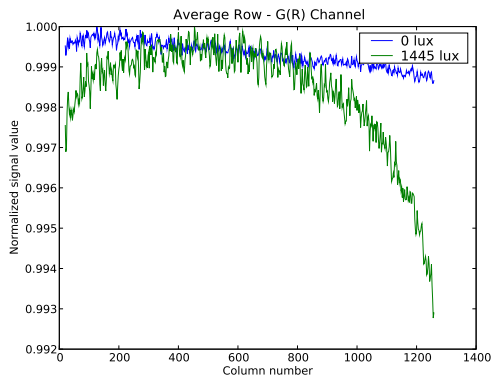Figure 35: Normalized average column of green pixels on red rows, two illuminations levels, ROI_1 A.1.

Figure 36: Normalized average row of green pixels on red rows, two illuminations levels, ROI_1 A.1.

As can be seen in figure 36 and 35, apart from a small horizontal and vertical gradient when the sensor is illuminated there seems to be a certain profile of the sensor response, with higher values in the middle, and lower at the edges. This is known as shading and usually refer to low frequency spatial variations in the sensors output. Potential sources include shading from the microlenses[7] [15].

This obviously affects the measured FPN, since the measure includes all spatial variation of the sensor response. Figure 36 shows an average row and apart from the shading component there is visible increase in the variability of the pixel response. This variability is what would appear as a stripy pattern as described in section 3.2.

---

[7]Tiny lenses on each pixel, used to increase the light collection efficiency.

Summary

The promise of a logarithmic image sensor with low FPN seems to hold true as the measurements show that the FPN is indeed quite small. The linear behavior also facilitates the use of flat-field correction (FFC) [6] to compensate for pixel gain and offset variations.
The temporal noise remains more or less constant when the illumination changes. The temporal noise is usually reduced by temporal averaging although it still limits the SNR at low illumination, this shown in section 4.3

4.3   Signal-to-noise Ratio

The aquired signal and temporal noise data from section 4.1.2 and section 4.2 was combined in order to plot the SNR as defined in section 3.3 as a function of illumination. This was also done using simulated data for a commercial integrating pixel type sensor at 1/33 s exposure time. A comparison of the respective SNR behaviors can be seen in figure 37.
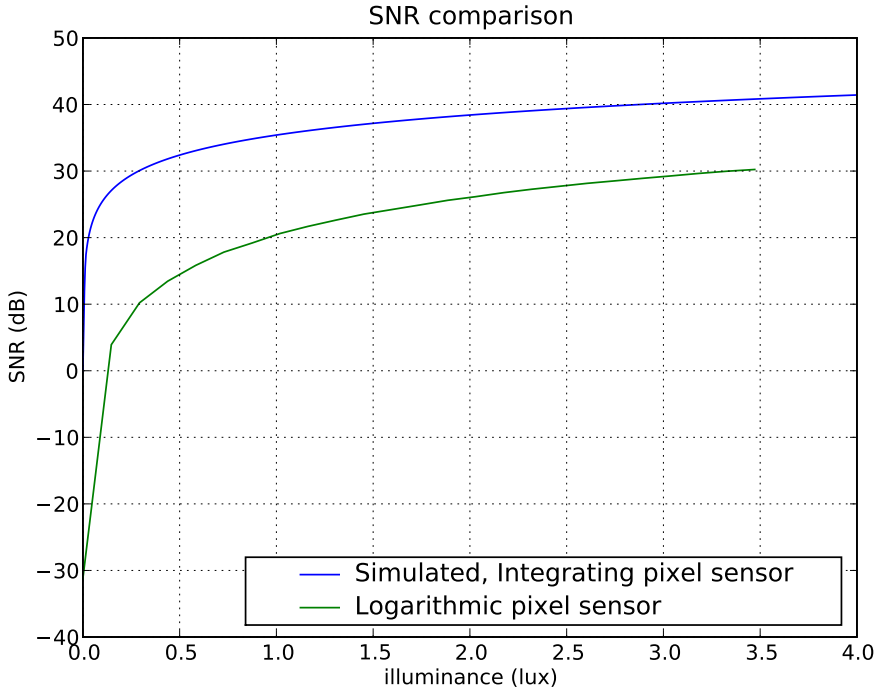

Figure 37: SNR comparison of logarithmic sensor and traditional integrating sensor.

As can be seen in figure 37, the SNR rises much faster for the traditional integrating linear pixel. This means that at low illumination levels the amount of noise will be higher for the logarithmic sensors, thus resulting in worse image quality.

4.4 Dynamic Range

The measurement was performed in accordance with the description in section 3.4. To remove both temporal noise and to compensate for intensity variations of the laser. 1000 images of the diffraction pattern were captured and averaged.

One issue during this test was that the laser was not able to saturate the sensor. Therefore it was not possible to measure the exact dynamic range, but only a lower bound of the dynamic range. Figure 38 shows a gray scale image of the diffraction pattern.

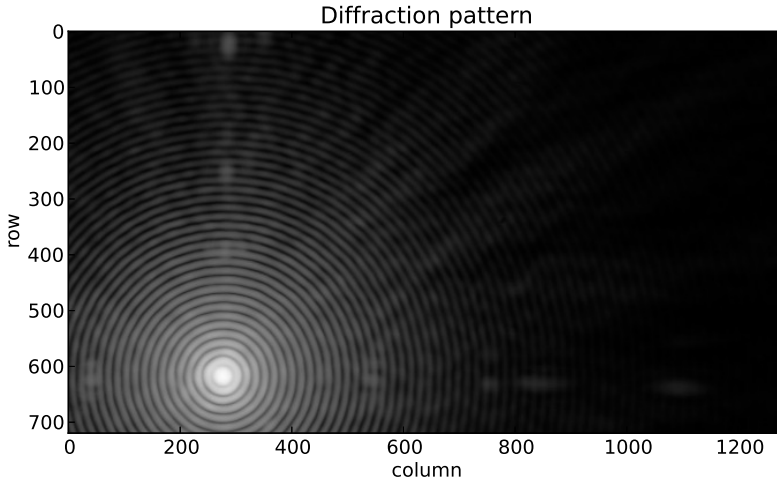Figure 38: Averaged image taken during laser diffraction test.

In the full scale image, 46 individual rings were counted which would lead to a dynamic range of 121.9dB. Alternatively a row intersecting the main peak can be extracted from figure 38. Assuming a constant temporal noise level of at most 11 (10.55) ADU as measured in section 4.2, the SNR of the extracted row can be plotted. This can be seen in figure 39.
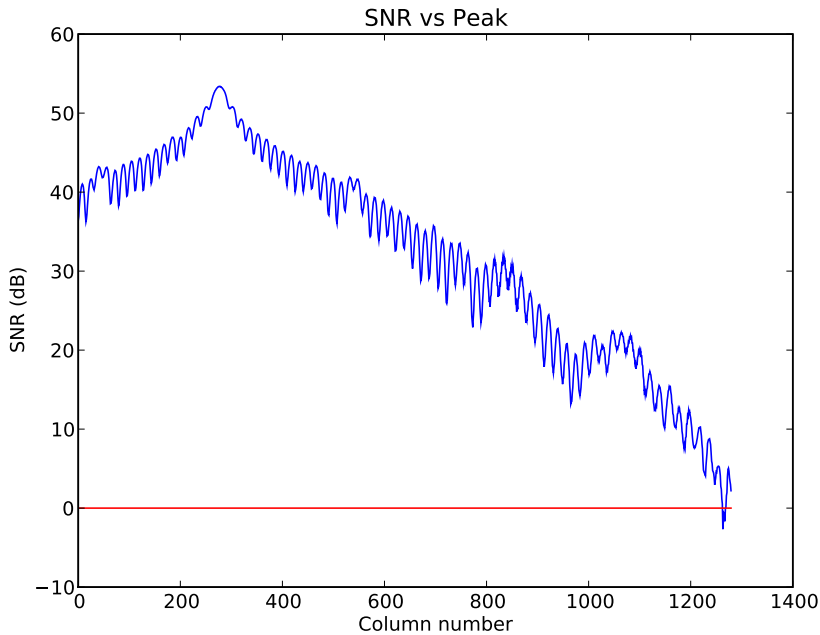
Figure 39: SNR of row intersecting the main peak of the diffraction pattern.

As can be seen in figure 39 all peaks appear to have a SNR above 1 (0dB). There are 58 peaks in total which would mean a dynamic range of 127.9dB.

To conclude, the sensor has a dynamic range of at lest 121.9dB or 127.9dB depending on what measure is used. However since the sensor didn't saturate it is not possible to state the total dynamic range, only a lower bound can be established.

For comparison, the data from a similar measurement performed on a multi-exposure type camera was received from Axis Communications AB, quoting a dynamic range of 110dB. This is clearly less, although it's not possible to claim that one is better than the other on dynamic range alone since this measure doesn't specify "where" the dynamic range is. For instance, in some circumstances it might be more important with low light sensitivity than a high saturation point.

4.5 Transient Response

As mentioned in section 3.5. A number of frames were acquired as the image sensor was illuminated using the setup described in section 2.5. The LED was repeatedly turned on and off to facilitate the recording of frames during the led illumination changes. The row averages were then computed for all frames. The resulting row averages for three consecutive frames at the point of the LED illuminations changes can be seen in figure 40.
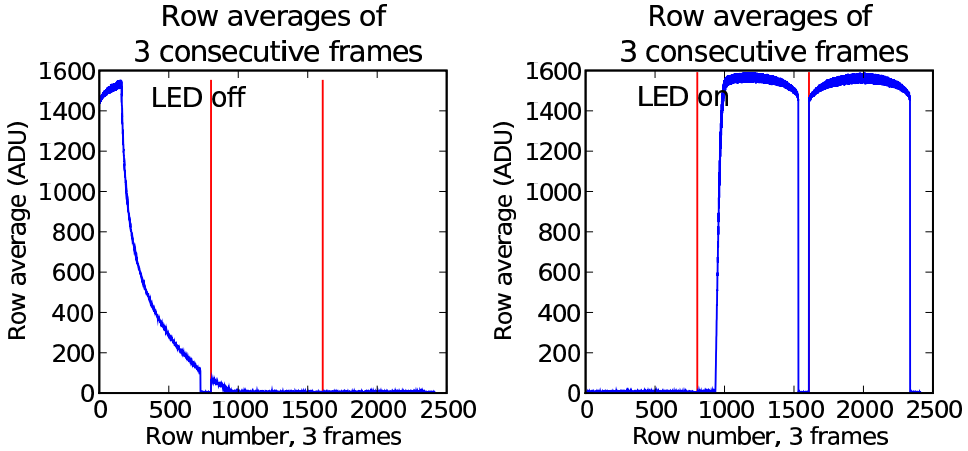
Figure 40: Average rows for three consecutive frames, for LED on and off.

The respective responses for when the LED was turned on and off were extracted for a number of different illumination levels. This can be seen in figure 41 and 42. Two different ND filter were used in the measurements, one with an optical density of 0.1 corresponding to approximately 80% transmittance, and one with an optical density of 0.5 corresponding to approximately 32% transmittance.

Figure 41: Normalized rise response versus read out row.

Figure 41 shows the read out row normalized with respect to the maximum read out value and the illumination profile of the LED. This was done with two different ND filters with an optical density of 0.1 and 0.5 respectively. As can be seen in the figure, the response of the measurement with the slightly less dark filter seems to reach the maximum illumination a bit faster.

The "rows" with value zero in the middle of the pictured response is what is known as Vblank, and is the time corresponding to a certain number of "empty" lines that are read out between frames. The fact that the Vblank appears to coincide for the two measurements is due to selection for easier comparison.
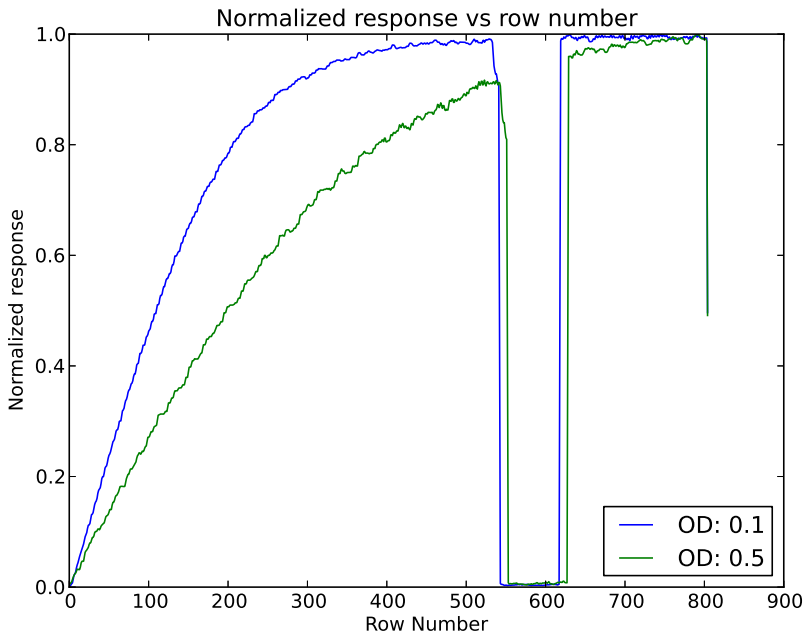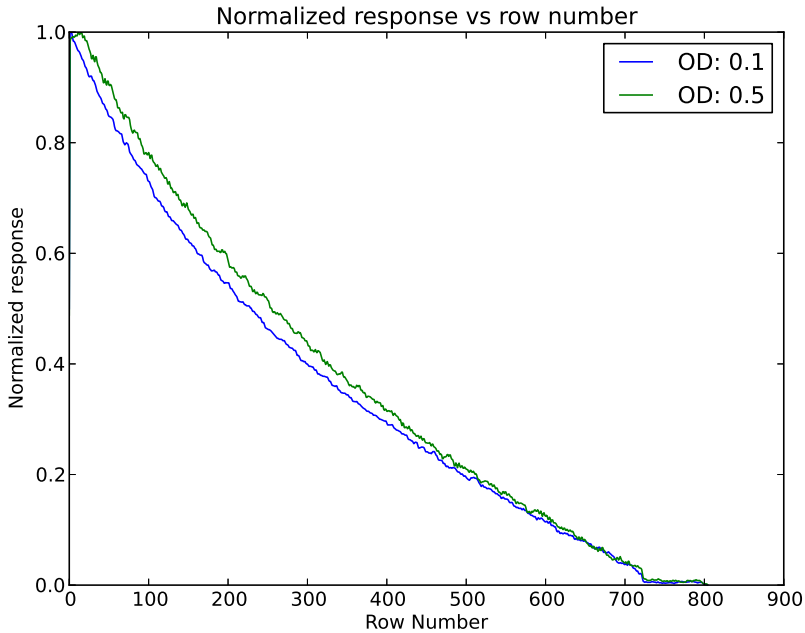
Figure 42: Normalized fall response versus read out row.

Figure 42 shows the read out row normalized with respect to the maximum read out value and the illumination profile of the LED. This was done with two different ND filter with an optical density of 0.1 and 0.5 respectively. Here the response is much more similar and it is not possible to conclude that one is faster than the other.

Summary

Studying the response when a LED was turned on, it seems that one can conclude that the response is indeed faster when the illumination level is higher.

It is also apparent that the response is different from the response of a traditional integrating image sensors described in section 3.5. Particularly in the sense that it is not symmetrical with respect to when the LED is turned on and off.

Since the read out signal is affected by both the rolling shutter effect and the pixel response, it is hard to conclude exactly how the different effects contribute to the response.

It is possible that the different response might render motion slightly different in some circumstances, especially in low light when the response is slower. This was evaluated with a simple test of imaging a rotating object at different illumination levels. This can be seen in figure 43.
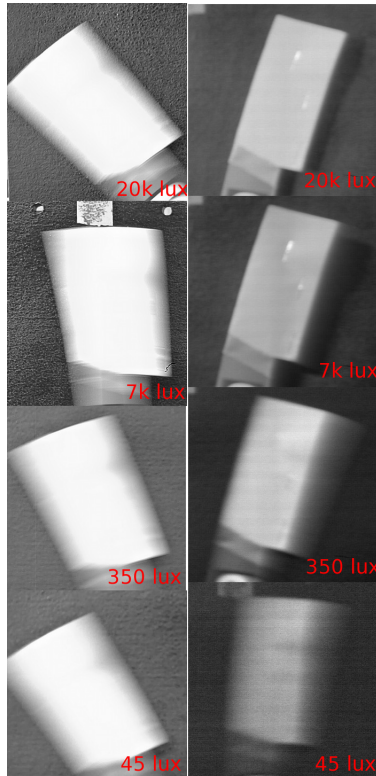
Figure 43: Images of object rotating at 30rpm at different illumination levels. Comparison with integrating sensor.

The images to the left were taken at 1/25 s exposure and as can be seen, the motion blur is independent of illumination and only depends on the exposure time. For the logarithmic sensor to the right, there is almost no motion blur at all at 20 000 lux but there is visible blur when the illumination is decreased. Additionally the rotating object is rotating counter clockwise and there seems to be more motion blur after the object than before it when captured by the logarithmic sensor. This could potentially be explained by the response seen in figure 41 and 42 as the fall response seems slower than the rise response.

With a linear integrating sensor the amount of motion blur can be regulated by choosing longer or shorter exposure times, altough there is always a tradeoff between the amount of noise and motion blur. With the logarithmic sensor it is not possible to choose between motion blur or noise, low illumination will always lead to motion blur.

5 Conclusions and Future Work

Conclusions

Reiterating the questions set up in section 1.5, the following results are worth calling attention to:

The sensor response does indeed follow a logarithmic law at high illumination levels. As the sensor was not saturated even by a laser it is probably fair to say that saturation of the sensor is not a problem when using a logarithmic sensor with this design.

As measured in section 4.2.2 the FPN is quite low, especially in the context of logarithmic CMOS sensors. This shows that the new design and the presence of a reset vastly improves the sensor performance. The temporal noise remains constant although it is quite high compared to common integrating sensors as shown in section 4.3. This limits the low light performance of the logarithmic sensor.

From the data in section 4.1.2, no obvious transition between linear and logarithmic mode can be seen and the response seems to be smooth over the entire usable range.

As shown in section 4.5, the fact that the sensor is not integrating does change certain behaviors, for instance motion blur. This thesis does not address all possible motion-related behavior differences and this is an area that might warrant more investigation.

The temperature measurements in section 2.3 have shown that the temporal noise stays constant and there is an increase in FPN. More alarming though, the dark signal seems extremely unstable with regard to temperature and would make a stable implementation hard to achive.
Aditional work is needed to fully understand the temperature dependent behavior of the sensor.

Outlook and Future Work

The prospect of using this type of logarithmic image sensors as an alternative WDR solution instead of various multiple exposures methods is interesting. The use of only one exposure or read out is an obvious advantage compared to the use of multiple exposure since it eliminates the issue of accurate motion representation.
Additionally there is no need for an exposure-algorithm that changes the exposures in different situations which is a nice feature, reducing the complexity of the imaging system.
The logarithmic response does present a number of challenges with regard to image processing though. Little or no work in the field of tone mapping[8] has been done specifically for the use with logarithmic image sensors. Some work related to correct color representation has been done [12] suggesting that this should be possible.

---

[8]Techniques for how to compress WDR images without loosing information.

References

[1] Key differences between rolling shutter and frame (global) shutter. `http://www.ptgrey.com/support/kb/index.asp?a=4&q=115`. Accessed: 2012-06-26.

[2] Noise sources in cmos image sensors. `http://www.stw.tu-ilmenau.de/~ff/beruf_cc/megatek/noise.pdf`, jan 1998. Accessed: 2012-06-26.

[3] Digital camera basics. `http://www.ni.com/white-paper/3287/en`, February 2012. Accessed: 2012-06-26.

[4] P.M. Acosta-Serafini, I. Masaki, and C.G. Sodini. A 1/3" vga linear wide dynamic range cmos image sensor implementing a predictive multiple sampling algorithm with overlapping integration intervals. *Solid-State Circuits, IEEE Journal of*, 39(9):1487 – 1496, sept. 2004.

[5] S.G. Chamberlain and J.P.Y. Lee. A novel wide dynamic range silicon photodetector and linear imaging array. *Electron Devices, IEEE Transactions on*, 31(2):175 – 182, feb 1984.

[6] Justin C. Dunlap, William C. Porter, Erik Bodegom, and Ralf Widenhorn. Dark current in an active pixel complementary metal-oxide-semiconductor sensor. *Journal of Electronic Imaging*, 20(1):013005, 2011.

[7] Yibing (Michelle) Wang et al. A high dynamic range cmos aps image sensor. `http://www.ericfossum.com/Publications/Papers/2001%20Program%20A%20High%20Dynamic%20Range%20CMOS%20APS%20Image%20Sensor.pdf`. Accessed: 2012-06-26.

[8] David Gardner. Characterizing digital cameras with the photon transfer curve. `http://www.couriertronics.com/docs/notes/cameras_application_notes/Photon_Transfer_Curve_Charactrization_Method.pdf`. Accessed: 2012-06-26.

[9] E. Hecht. *Optics*. Addison-Wesley, 2002.

[10] John D. Hunter. Matplotlib: A 2d graphics environment. *Computing In Science & Engineering*, 9(3):90–95, May-Jun 2007.

[11] Eric Jones, Travis Oliphant, Pearu Peterson, et al. SciPy: Open source scientific tools for Python. `http://www.scipy.org/`, 2001–. Accessed: 2012-06-26.

[12] D. Joseph and S. Collins. Modelling, calibration and rendition of colour logarithmic cmos image sensors. In *Instrumentation and Measurement Technology Conference, 2002. IMTC/2002. Proceedings of the 19th IEEE*, volume 1, pages 49 – 54 vol.1, 2002.

[13] S. Kavadias, B. Dierickx, D. Scheffer, A. Alaerts, D. Uwaerts, and J. Bogaerts. A logarithmic response cmos image sensor with on-chip calibration. *Solid-State Circuits, IEEE Journal of*, 35(8):1146 –1152, aug 2000.

[14] A. D Kerr. The iso definition of the dynamic range of a digital still camera. `http://dougkerr.net/Pumpkin/articles/ISO_Dynamic_range.pdf`, feb 2008. Accessed: 2012-06-26.

[15] J. Nakamura. *Image Sensors and Signal Processing for Digital Still Cameras*. Optical Science and Engineering. Taylor & Francis, 2006.

[16] P.J.W. Noble. Self-scanned silicon image detector arrays. *Electron Devices, IEEE Transactions on*, 15(4):202 – 209, apr 1968.

[17] Travis E. Oliphant. *Guide to NumPy*. Provo, UT, March 2006.

[18] J.M. Palmer and B.G. Grant. *The Art of Radiometry*. [Press monograph. SPIE Press, 2010.

[19] E. Reinhard. *High Dynamic Range Imaging: Acquisition, Display, and Image-Based Lighting*. Morgan Kaufmann Series in Computer Graphics and Geometric Modeling. Elsevier, 2006.

[20] N. Ricquier and B. Dierickx. Pixel structure with logarithmic response for intelligent and flexible imager architectures. In *Solid State Device Research Conference, 1992. ESSDERC '92. 22nd European*, pages 631 –634, sept. 1992.

[21] Orit Skorka and Dileepan Joseph. Toward a digital camera to rival the human eye. *Journal of Electronic Imaging*, 20(3):033009, 2011.

[22] S. Sugawa, N. Akahane, S. Adachi, K. Mori, T. Ishiuchi, and K. Mizobuchi. A 100 db dynamic range cmos image sensor using a lateral overflow integration capacitor. In *Solid-State Circuits Conference, 2005. Digest of Technical Papers. ISSCC. 2005 IEEE International*, pages 352 –603 Vol. 1, feb. 2005.

[23] G. van Rossum and F.L. Drake (eds). *Python Reference Manual*. Virginia, USA, 2001.

[24] O. Yadid-Pecht and E.R. Fossum. Wide intrascene dynamic range cmos aps using dual sampling. *Electron Devices, IEEE Transactions on*, 44(10):1721 – 1723, oct 1997.

[25] David X. D. Yang and Abbas El Gamal. Comparative analysis of snr for image sensors with enhanced dynamic range. volume 3649, pages 197–211. SPIE, 1999.

[26] D.X.D. Yang, A.E. Gamal, B. Fowler, and H. Tian. A 640 times;512 cmos image sensor with ultrawide dynamic range floating-point pixel-level adc. *Solid-State Circuits, IEEE Journal of*, 34(12):1821 –1834, dec 1999.

[27] Bogdan Arion Yang Ni, YiMing Zhu. A 768x576 logarithmic image sensor with photodiode in solar cell mode. Accessed: 2012-06-26, 2011.

A   Appendix A - Measurement Specifications

A.1   Sphere Measurement Specifications.

This measurement was conducted using the Integrating Sphere described in section 11.

Environment temperature: $23°C$

Sphere lamp intensity: 16%

1. The image sensor was mounted on the sphere without any optics or filter.

2. The image sensor was turned on and allowed to run for 60 minutes to reach a stable operating temperature.

3. The integrating sphere attenuator was gradually closed. At each setting 100 frames were grabbed from the image sensor and the sphere radiometer values were recorded. After each frame grab of illuminated frames, the sphere lamp was turned off and 100 completely dark frames were captured. This, to be able to correct for black level drift due to temperature variations.

Attenuator (%)	Radiometer (A)	Attenuator (%)	Radiometer (A)
100	9.2718e-5	0.24	2.2275e-7
75	6.7899e-5	0.23	2.1345e-7
50	4.5414e-5	0.22	2.0414e-7
36	3.2704e-5	0.21	1.9486e-7
25	2.2751e-5	0.20	1.8561e-7
19	1.7286e-5	0.19	1.7640e-7
12	1.0951e-5	0.18	1.6712e-7
9	8.2250e-6	0.17	1.5797e-7
6	5.4958e-6	0.16	1.4879e-7
4	3.6706e-6	0.15	1.3955e-7
3	2.7561e-6	0.14	1.3020e-7
2	1.8414e-6	0.13	1.2096e-7
1	9.2425e-7	0.12	1.1174e-7
0.9	8.3150e-7	0.11	1.0248e-7
0.8	7.3943e-7	0.10	9.3221e-8
0.7	6.4775e-7	0.09	8.3938e-8
0.6	5.5537e-7	0.08	7.4599e-8
0.5	4.6283e-7	0.07	6.5365e-8
0.4	3.7076e-7	0.06	5.6052e-8
0.3	2.7818e-7	0.05	4.6741e-8
0.29	2.6884e-7	0.04	3.7429e-8
0.28	2.5956e-7	0.03	2.8102e-8
0.27	2.5038e-7	0.02	1.8776e-8
0.26	2.4125e-7	0.01	9.4255e-9
0.25	2.3198e-7	0	0